www.czasopisma.pan.pl PAN POLSKA AKADEMIA NAUK www.journals.pan.pl

Arch. Metall. Mater., Vol. 61 (2016), No 2B, p. 1249–1254

DOI: 10.1515/amm-2016-0206

M. STOPYRA*#, D. NIEMIEC*, G. MOSKAL*

SYNTHESIS, CHARACTERIZATION AND THERMAL DIFFUSIVITY OF HOLMIUM AND PRASEODYMIUM ZIRCONATES

$A_2B_2O_7$ oxides with pyrochlore or defected fluorite structure are among the most promising candidates for insulation layer material in thermal barrier coatings. The present paper presents the procedure of synthesis of holmium zirconate $Ho_2Zr_2O_7$ and praseodymium zirconate $Pr_2Zr_2O_7$ via Polymerized-Complex Method (PCM). Thermal analysis of precursor revealed that after calcination at relatively low temperature (700°C) fine-crystalline, single-phase material is obtained. Thermal diffusivity was measured in temperature range 25-200°C, $Ho_2Zr_2O_7$ exhibits lower thermal diffusivity than $Pr_2Zr_2O_7$. Additionally, $PrHoZr_2O_7$ was synthesized. The powder in as-calcined condition is single-phase, but during the sintering decomposition of solid solution took place and Ho-rich phase precipitated. This material exhibited the best insulating properties among the tested ones.

Keywords: pyrochlores, synthesis, polymerized-complex method, holmium zirconate, praseodymium zirconate, thermal diffusivity

1. Introduction

Some of binary oxides with general formula $A_2B_2O_7$ exhibit pyrochlore-type of crystal structure. It is usually described as derived from fluorite by removing oxygen anions at 8a site and ordering in cation sub-lattice. As a consequence, ordered pyrochlore structure (space group Fd-3m) can be distinguished from fluorite (space group Fm-3m) by the superlattice coming from ordering both in anionic and cationic arrays. The A-site is occupied by larger, trivalent and 8-coordinated cations, typically rare earth elements. The B cations are smaller, tetravalent and 6-coordinated, usually transition metals, i. a. Zr, Ti, Hf [1-3]. Therefore, there are a lot of possible combinations of chemical compositions for a pyrochlore-type of oxides, but the ordered structure occurs only for the ones in which the ratio of ionic radii $r = r_A/r_B$ is in the range between 1,46 and 1,78. In case of zirconates pyrochlore structure is stable from La to Gd. In case of smaller lanthanides, the superlattice does not occur, but the stoichiometry is still the same, due to the lack of 1/8 oxygen ions in relation to MO_2 fluorite. Hence, these compound are usually referred to as defected fluorites or disordered pyrochlores.

The methods for synthesis of pyrochlores used in available literature can be divided into two main groups: conventional ceramic process and wet-chemical methods. The former, often called Solid-State-Reaction (SSR) the input materials are oxide powders, which are weighed in order to obtain certain stoichiometry, then mixed and homogenized and finally sintered. This method is relatively easy, hence it is commonly used [4], however its disadvantage is inhomogeneity of the final product in terms of chemical and phase composition. It is caused by the fact that the interaction between the different powder grains takes place on their interface so the efficiency of synthesis process is governed by the diffusion. In order to provide high homogeneity it is necessary to carefully prepare the mixture, which is usually done by the high-energy ball milling. This process is followed by sintering process, during which the new oxide is synthesized. In case of RE zirconates synthesis temperature often exceeds 1500°C and the time can be more than 24 h. Moreover, even nano-metric powders have the tendency to form agglomerates with more complex shape, which are hard to break-up during milling, that is why the milling-synthesis cycle is sometimes repeated several times [5].

The wet-chemical methods include i.a. co-precipitation [6], sol-gel [7] and hydrothermal method [8]. The commonly emphasized advantage of sol-gel type of methods is homogeneity of synthesized compound and precise control over its stoichiometry. On the other hand, its major drawback could be the high price of substrates. The polymerized-complex method (PCM) also belongs to the wet-chemical methods, however it is different from typical sol-gel methods, as gel is obtained from the solution, not from the colloid [9].

Owing to the unique crystal structure and wide range of possible chemical compositions, $A_2B_2O_7$ pyrochlores exhibit many interesting properties, including extremely low thermal conductivity (ca. 30% lower than 8YSZ), which makes them potential candidates for insulation layer in modern thermal barrier coatings [10]. Some of them, e.g. $Gd_2Zr_2O_7$ have been already widely studied in terms of their thermal properties [11], however

* SILESIAN UNIVERSITY OF TECHNOLOGY, FACULTY OF MATERIALS ENGINEERING AND METALLURGY, 8 KRASIŃSKIEGO STR., 40-019 KATOWICE, POLAND

Corresponding author: michal.stopyra@polsl.pl

the data concerning other rare earth zirconates, including Ho and Pr is still lacking. Moreover, it was already recognized, that introducing of crystal lattice defects is conducive to improving thermal insulation. This phenomena provided the new direction in the studies on insulating properties of rare earth pyrochlores.

The aim of present work was synthesis, characterization of structure and thermal properties of $Ho_2Zr_2O_7$ and $Pr_2Zr_2O_7$, additionally the compound with intermediate composition $PrHoZr_2O_7$ was investigated.

2. Materials and experimental procedure

The materials for the research were obtained using polymerized-complex method and then their structure and insulating properties were studied.

Synthesis

RE^{3+} cations were introduced as nitrates hydrates $Pr(NO_3)_3 \cdot 6H_2O$ (99,99%, Onyx-Met) and $Ho(NO_3)_3 \cdot 5H_2O$ (99,99%, Onyx-Met), and Zr^{4+} as nitrate $Zr(NO_3)_4$ (99,99%, Onyx-Met). The substrates were weighed to obtain the molar ratio $RE^{3+}/Zr^{4+} = 1$ and dissolved in distilled water. Citric acid (CA) was added in $CA/(RE^{3+} + Zr^{4+}) = 4$ molar ratio and ethylene glycol (EG) in EG/CA = 1 molar ratio. The transparent solution was magnetically stirred at ca. 80°C/2h in order to obtain homogeneous distribution of metalo-citrate complexes. Then the solvents were evaporated and glassy resin was formed, which after drying at ca. 300°C was crushed in mortar. The obtained powder is referred to as precursor.

The calcination was conducted in muffle furnace in static air. Powders were sintered into 12 mm diameter pellets in "Degussa" press at 1300°C/4h with additional load 15 MPa in vacuum.

Characterization

The obtained precursor were investigated using differential thermal analysis and thermogravimetry methods (DTA/TG, Setaram SetSys 16 apparatus). The experiment was carried out in synthetic air atmosphere in the temperature range 25-1300°C, with the heating rate 5°C/s.

The morphology of powders and sinters was analyzed using scanning electron microscope (SEM, Hitachi S-3400N) equipped with energy-dispersive spectrometer (EDS, Thermo Noran System Six) for microanalysis of chemical composition. The phase analysis was carried out using X-ray diffraction (XRD, Jeol JDX-7S).

The sinters' density (ρ) was measured in accordance to Archimedes principle using laboratory scale with accuracy 0,0001 g, the measurement uncertainty was calculated as a total differential. Thermal diffusivity (α) was measured using laser-flash method (LFA, Netsch LFA 427) in the temperature range 50-200°C. The samples were spray-coated with graphite and Ar 5.0 was used as protective gas. Cape-Lehman model was used to calculate thermal diffusivity. Three measurements were made in each temperature and the mean values with standard deviation were presented. Specific heat was calculated based on Neumann-Kopp rule. Thermal conductivity (κ') was calculated:

$$\kappa' = \alpha \cdot \rho \cdot C_p \tag{1}$$

As the samples contained micropores, the measured values were adjusted using following equation [12]:

$$\frac{\kappa'}{\kappa} = \left(1 - \frac{4}{3}\varphi\right)^{-1} \tag{2}$$

Where: κ – thermal conductivity of fully dense material; κ' – thermal conductivity calculated using formula (1); φ – normalized porosity (pores volume fraction). This formula was developed for yttria-stabilized zirconia but was also used for RE zirconates [13].

3. Results and discussion

The DTA/TG curves for Pr and Ho zirconates are presented in Fig. 1. The decomposition of organic gel can be divided into 3 stages. At first, up to ca. 200°C the mass loss is due to the dehydration. The strong exothermal effect accompanied by the biggest mass loss (ca. 60%) is attributed to pyrolysis of organic compounds formed during the synthesis process. 2 and 3 exothermal peaks can be distinguished in case of Ho and Pr zirconates, respectively, which suggests that the pyrolysis of investigated precursors has stepwise character, the endset temperatures for the last peaks were determined at 474°C ($Ho_2Zr_2O_7$) and 498°C

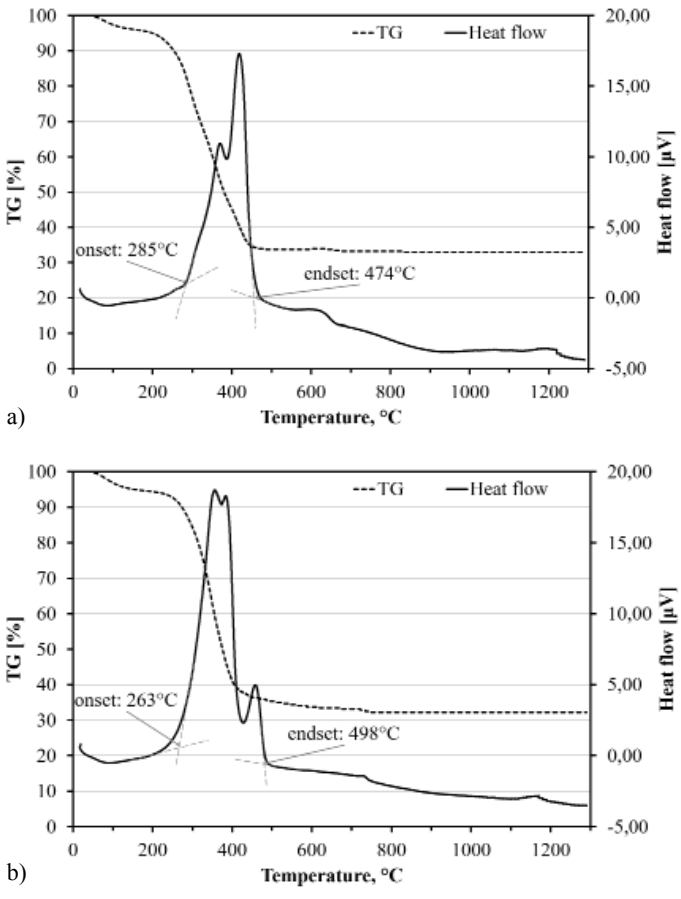

Fig. 1. DTA/TG curves for precursors: $Ho_2Zr_2O_7$ (a) and $Pr_2Zr_2O_7$ (b)

($Pr_2Zr_2O_7$). Above these temperatures small, gradual mass loss can be still observed which can be attributed to burning out of residue organics. Based on these results the calcination temperature 700°C was determined.

The results of XRD analysis for the as-calcined powders are presented in Fig. 2. The broadening of the peaks is due to the nano-sized crystallites, which is typical for the materials synthesized with via wet-chemical methods. No sign of presence foreign phases could be observed. Moreover, in such fine-crystalline material it is impossible to distinguish the small peaks attributed to superlattice in $Pr_2Zr_2O_7$ (311, d = 3,2200, 2Θ = 27,65°; 331: d = 2,4400, 2Θ = 36,80°; 511, d = 2,0560, 2Θ = 44,00°) which indicates the obtained powder has defected fluorite type of structure (Fm-3m), similarly to $Ho_2Zr_2O_7$ and $PrHoZr_2O_7$.

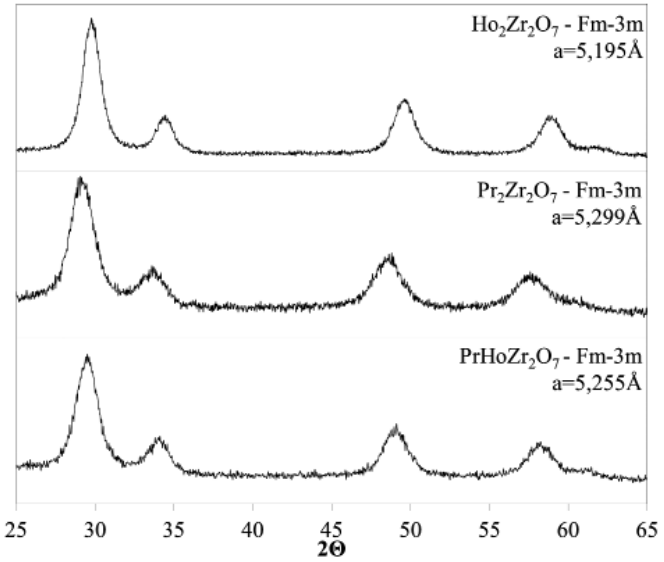

Fig. 2. XRD spectra for the as-calcined at 700°C/3h powders

The morphology of obtained powders is presented in Fig. 3. The grains have irregular shape and size in the range from few to ca. 30 μm. It is due to the synthesis process – after formation of the gel, hard agglomerates are formed. This is less favorable morphology in terms of densification during sintering than e.g. in case of high energy ball-milled powders. However, they already have designed chemical and phase composition, thus they do not need any further homogenization via such process as ball-milling.

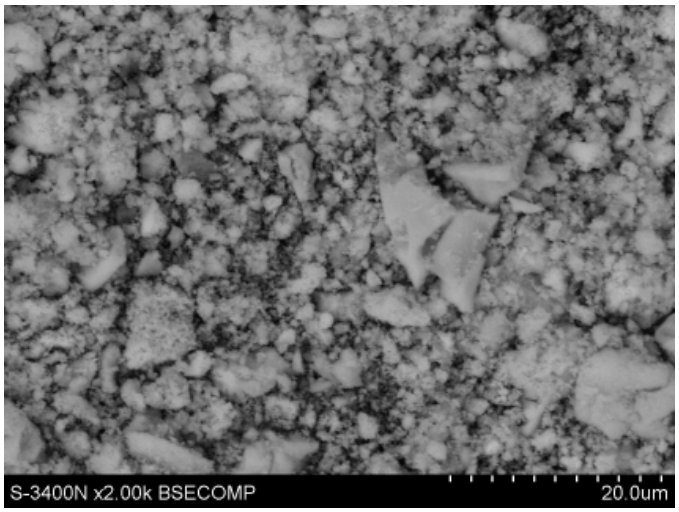

Fig. 3. Typical morphology of powder obtained via PCM, after crushing and calcination

The EDS results (Fig. 4, tab. 1) indicate that there is good agreement between the content of specific elements and the assumed stoichiometry. As the EDS method is not suitable for quantitative analysis of light elements, the presented oxygen content is calculated on the assumption that all of it forms stoichiometric oxides Pr_2O_3, Ho_2O_3 and ZrO_2. In the case of $PrHoZr_2O_7$ the deviation of the perfect stoichiometric ratios (Pr/Ho = 0,81, (Pr + Ho)/Zr = 0,92) could be rather attributed to the measurement uncertainty than non-stoichiometry. It is indicated by the lattice parameters (Fig. 2) – the value calculated for $PrHoZr_2O_7$ is close to mean value of Pr and Ho zirconates' parameters, which suggest the Pr/Ho ratio should be close 1, in accordance to Vagard's law.

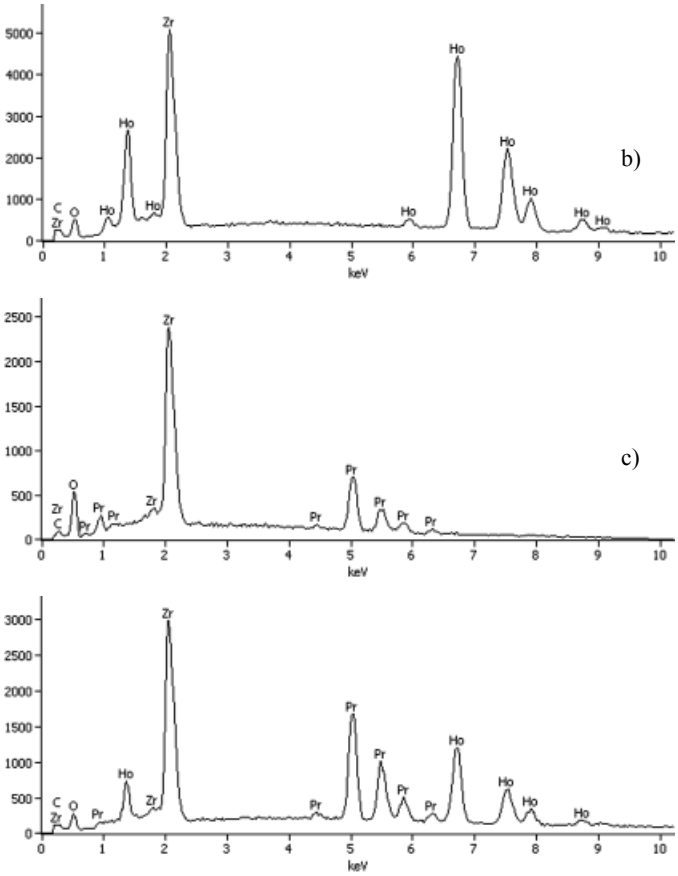

Fig. 4. EDS spectra from the obtained powders: $Ho_2Zr_2O_7$ (a), $Pr_2Zr_2O_7$ (b) and $PrHoZr_2O_7$ (c)

TABLE 1

Average chemical composition obtained from EDS analysis for powders after calcination, $\%_{at.}$

	O (s)	Zr	Pr	Ho
$Ho_2Zr_2O_7$	63,6	18,1	–	18,3
$Pr_2Zr_2O_7$	63,6	17,8	18,7	–
$PrHoZr_2O_7$	63,8	18,9	7,8	9,6

Fig. 5 presents the XRD results for the as-sintered pellets. Both $Pr_2Zr_2O_7$ and $Ho_2Zr_2O_7$ exhibit single phase composition: defected fluorite in case of Ho zirconate, as r_{Ho}/r_{Zr} = 1,39 and ordered pyrochlore in case of Pr zirconate.(r_{Pr}/r_{Zr} = 1,54). Thermally activated ordering transformation from defected fluorite to ordered pyrochlore resulted in occurrence of new peaks, attributed to superlattice and marked with "x" in Fig. 5. Both of these oxides are has single-phase composition, the doubled peaks at high 2θ in $Ho_2Zr_2O_7$ can be attributed to Kα2 line, which becomes more visible at high angles as the result of crystallite growth and peak narrowing.

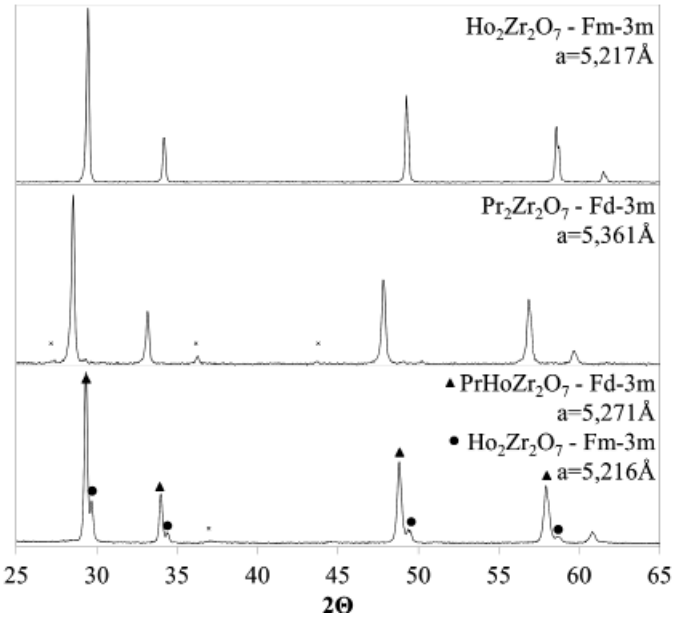

Fig. 5. XRD spectra for the materials in as-sintered condition (lattice parameters in case of Fd-3m structure are divided by 2 for better comparison)

The $PrHoZr_2O_7$ can be considered solid solution of Pr and Ho zirconates in 1:1 ratio. From the results of XRD analysis it can be concluded that this solution is metastable. Despite the same type of crystal strucuture these zirconates form solid solution with limited solubility which is due to big difference in the ionic radii of Pr (1.126Å) and Ho (1.015Å). Even though Pr and Ho cations were homogeneously distributed in as-calcined powder, decomposition of solid solution by precipitation of $Ho_2Zr_2O_7$ (as indicated by the position of new peaks) occurs during sintering. It should be also noted that this phenomenon takes place probably in nano-areas as no sign of chemical inhomogeneity could be seen in the microstructure of sintered $PrHoZr_2O_7$ (Fig. 6). Hence, even though the sinter has multi-phase composition, its structure is of completely different character than in case of materials synthesized via SSR process, where the presence of areas enriched with one of constituent oxides results from inhomogeneity of input mixture and locally excessive content of one of substrates during the synthesis.The precipitation of $Ho_2Zr_2O_7$ resulted in decrease of Ho content in the remaining solid solution which increased r_{RE}/r_{Zr} ratio (where r_{RE} is weighed mean value of r_{Pr} and r_{Ho}) and drove the system from defected fluorite towards ordered pyrochlore. As a consequence, small peak attributed to superstructure (331) occurred. The separate comment should be made on the change in lattice parameters – the peaks from Pr-rich solid solution shifted towards higher angles (namely, $Ho_2Zr_2O_7$

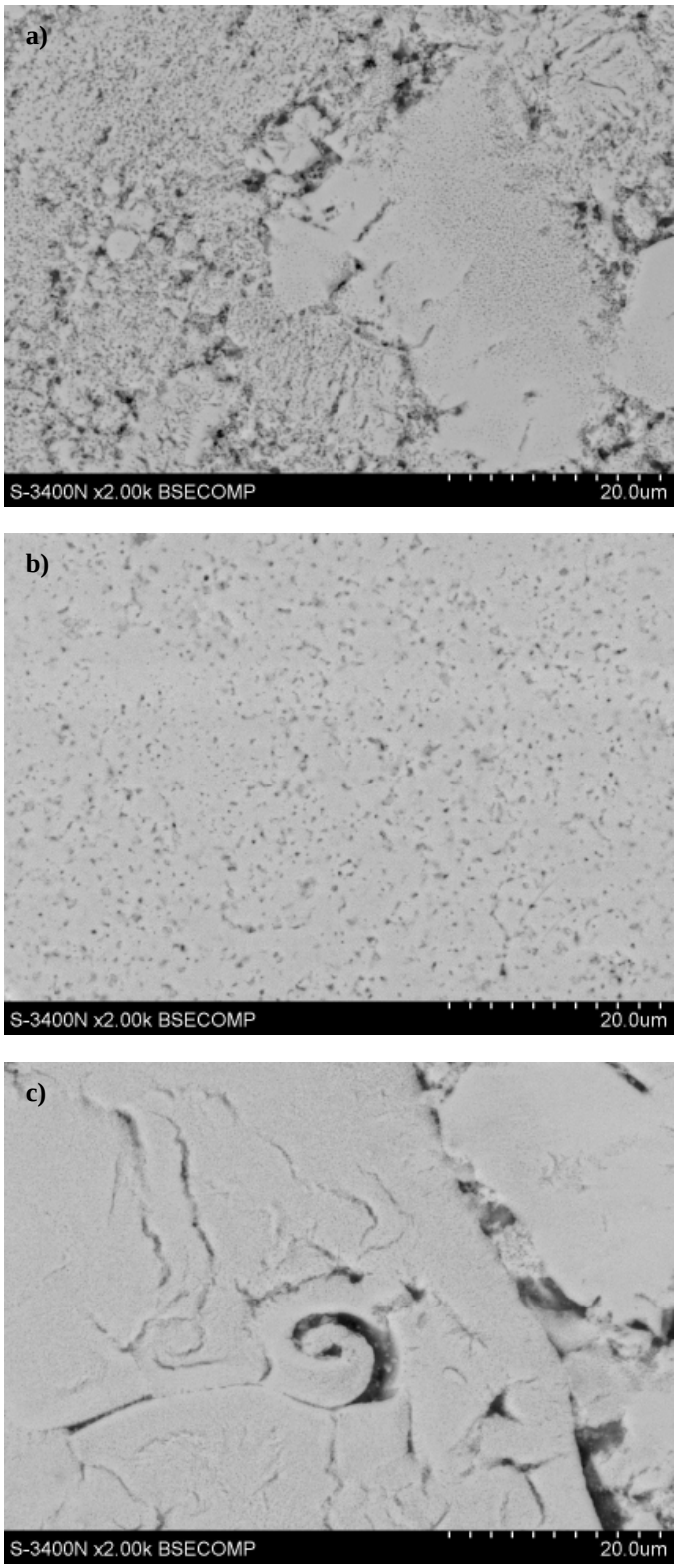

Fig. 6. Morphology of obtained sinters: $Ho_2Zr_2O_7$ (a), $Pr_2Zr_2O_7$ (b) and $PrHoZr_2O_7$ (c)

side) despite the precipitation of $Ho_2Zr_2O_7$. Assuming the lattice parameter changes linearly with the content of substitution cation, the calculated content of Ho/Zr ratio is 63,5/36,5 instead of 50/50. This may be result of formation of anti-site defects [14].

Tab. 2 presents the results of density measurements. Theoretical density of $PrHoZr_2O_7$ was calculated assuming its value is in the middle between $Pr_2Zr_2O_7$ and $Ho_2Zr_2O_7$.

TABLE 2

The pores volume fraction (φ) of obtained sinters calculated on the basis of density measured in accordance to Archimedes principle (ρ) and theoretical density (ρ_T)

Sample	ρ, g/cm^3	ρ_T, g/cm^3	φ
$Ho_2Zr_2O_7$	5,601 ±0,006	7,29	0,232 ±0,001
$Pr_2Zr_2O_7$	5,049 ±0,004	6,28	0,196 ±0,001
$PrHoZr_2O_7$	5,320 ±0,005	6,76	0,212 ±0,001

Fig. 7 presents the results of measured thermal diffusivity with standard deviation as measurement uncertainty (if the error bars are not visible, standard deviation is smaller than the marker size). $Ho_2Zr_2O_7$ exhibits ca. 0,07 mm^2/s lower thermal diffusivity than $Pr_2Zr_2O_7$ in whole temperature range. This may be a result of more efficient phonon scattering on point defects due to the bigger mass fluctuation in Ho zirconate, as the atomic masses of Pr, Ho and Zr are 164,93, 140,91 and 91,22, respectively. However, because of higher atomic mass and lower ionic radius, Ho zirconates has higher density, which increases thermal conductivity.

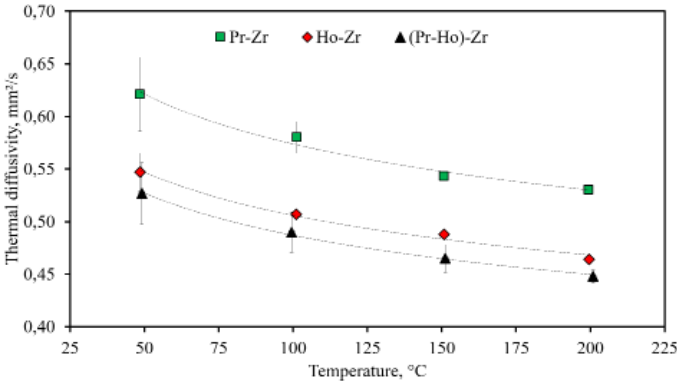

Fig. 7. Thermal diffusivity of obtained materials

$PrHoZr_2O_7$ exhibited the lowest thermal diffusivity (ca. 0,02 mm^2/s lower than $Ho_2Zr_2O_7$ in the whole temperature range). This difference may seem not significant, especially considering dispersion of the results. However, taking into consideration that $Ho_2Zr_2O_7$ has higher density and higher porosity, even this small difference indicates that $PrHoZr_2O_7$ exhibits superior insulating properties over Ho zirconate. Fig. 8 presents calculated thermal conductivity ($\kappa = C_p \cdot \alpha \cdot \rho$) of investigated materials.

Specific heat was calculated using literature data for constituent oxides [15,16], based on Neumann-Kopp law. It was

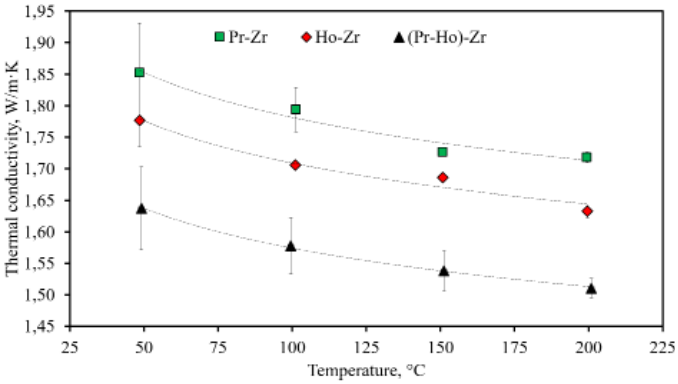

Fig. 8. Calculated thermal conductivity of obtained materials (error bars include both α and ρ uncertainty)

reported [17-19] that such calculations are in good agreement with measured values of heat capacity in RE zirconates. The relative change of density in 50-200°C range is negligible (~0,35%). Due to the differences in porosity, presented values of thermal conductivity were adjusted using (2) formula. Estimated thermal conductivity of $PrHoZr_2O_7$ is ~8% lower than of $Ho_2Zr_2O_7$ and ~11% lower than of $Pr_2Zr_2O_7$ in whole temperature range These results indicate strong phonon scattering effect in case of Pr-Ho zirconate. This is the result of the presence of point defects due to cation substitution. It is also possible that increase in insulating properties is enhanced by the presence of other defects – phase boundaries formed as a result of decomposition of solid solution and precipitation of Ho-rich phase. Point defects are very efficient phonon scattering centers, especially in materials with ultra-low thermal conductivity, where the mean phonon free path is less than 1 nm [13]. It was already recognized that maximization of the difference in ionic radii and atomic masses of substituted cations is conducive to reduction of thermal conductivity [13]. Moreover, the minimum thermal conductivity is usually expected at equimolar ratio of substituted cations where the defect concentration is the highest [13,20]. However, in case of $PrHoZr_2O_7$ this phenomenon was not used in full extent. Because of large difference between Ho^{3+} and Pr^{3+} ionic radii, the heavily defected single phase solid solution transformed into mixture of Ho-rich and Pr-rich phases with lower defect concentration. In turn, plane defects, namely pyrochlore-fluorite phase boundaries were formed. Grain boundaries and phase boundaries are usually considered less effective in terms of phonon scattering, because crystallite size in sintered ceramics is typically higher by orders of magnitude than mean phonon free path. Hence, in many works, e.g. [13,20] the influence of grain boundaries is considered negligible. However, it was also reported [21] that pyrochlore-fluorite boundaries might decrease thermal conductivity, as well as grain boundaries in different materials [22-24], including pyrochlore and fluorite-related [25]. More detailed studies are planned in future to explain the differences in thermal properties of dual phase RE zirconates.

4. Conclusions

Praseodymium and holmium zirconates and their 1:1 solid solution were successfully synthesized via PCM process. This method allows to obtain ceramic materials with high structural homogeneity and good control over the compound stoichiometry. Based on DTA/TG results calcination temperature was set at 700°C and after this process nano-crystalline, single-phase powders with no impurities were obtained. After sintering $Ho_2Zr_2O_7$ exhibits defected fluorite structure and $Pr_2Zr_2O_7$ – ordered pyrochlore structure. In case of $PrHoZr_2O_7$, due to precipitation of Ho-rich phase, the remaining Pr-rich solid solution undergoes disorder-order transition.

$Ho_2Zr_2O_7$ has lower thermal diffusivity than $Pr_2Zr_2O_7$ and $PrHoZr_2O_7$ exhibits the lowest thermal diffusivity among investigated materials. It is caused by the presence of point defects but it is possible that the presence of phase boundaries also contributed to this effect. More detailed investigation on this topic will be performed in future.

Acknowledgements

This work was supported by Institute of Materials Science of Silesian University of Technology, as a part of Statutory Research no BK220/RM3/2015 (11/030/BK-15/0025).

REFERENCES

[1] M.A. Subramanian, et al., Solid State Chem. **15**, 55 (1983).
[2] M. Toshihiroet al., Solid State Ionics **40-41**, 357 (1990).
[3] http://abulafia.mt.ic.ac.uk/shannon/ptable.php.
[4] W. Pan, et al., Thermochim. Acta **455**, 16 (2007).
[5] X. Xie, et al., J. Eur. Ceram. Soc. **31**, 1677 (2011).
[6] H. Chen, et al., J. Alloy. Compd. **480**, 843 (2009).
[7] S. Wang, et al., J. Eur. Ceram. Soc. **35**, 105 (2015).
[8] A.F. Redkin, et al., Phys. Chem. of Minerals **40**, 733 (2013).
[9] M. Kakihana, et al., J. Appl. Phys. **71**, 3904 (1992).
[10] J. Wu, et al., J. Am. Ceram. Soc. **35**, 3013 (2002).
[11] G. Moskal, et al., J. Eur. Ceram. Soc. **32**, 2025 (2012).
[12] K.W. Schlichting, et al., J. Mater. Sci. **36**, 3003 (2001).
[13] C.L. Wan, et al., Phys. Rev B **74**, 144109 (2006).
[14] A.V. Shlyakhtina, et al., Solid State Ionics **176**, 2297 (2005).
[15] G. Adachi, N. Imanaka, Z.C. Kang (Eds.), Binary Rare Earth Oxides, 2005 Springer
[16] T. Tojo, et al., J. Chem. Thermodyn. **31**, 831 (1999).
[17] Z.G. Liu, et al., J. Alloy. Compd. **475**, 21 (2009).
[18] O. Fabrichnaya, et al., Thermochim. Acta **558**, 74 (2013).
[19] Y. Zhang, et al., Mater. Res. Bull **64**, 175 (2015).
[20] C. Wan, et al., J. Am. Cer. Soc. **94**, 592 (2011).
[21] K.H. Kwak, et al., Mater. Lett. **65**, 2937 (2011).
[22] A.D. McConnel, et al., Annual Rev. Heat Transfer **14**, 129 (2005).
[23] S. Fayette, et al., J. Eur. Ceram. Soc. **20**, 297 (2000).
[24] D. Smith, et al., J. Am. Cer. Soc. **86**, 105 (2003).
[25] H. Chen, et al., J. Alloy. Compd. **480**, 843 (2009).